AIAA JOURNAL
Vol. 56, No. 5, May 2018

Azimuthal Variation of Instabilities Generated on a Flared Cone by Laser Perturbations

Amanda Chou*
NASA Langley Research Center, Hampton, Virginia 23681
and
Steven P. Schneider†
Purdue University, West Lafayette, Indiana 47907

DOI: 10.2514/1.J056419

To study the azimuthal development of boundary-layer instabilities, a controlled, laser-generated perturbation was created in the freestream of the Boeing/U.S. Air Force Office of Scientific Research Mach 6 Quiet Tunnel. The freestream perturbation convected downstream in the wind tunnel to interact with a flared-cone model. The flared cone is a body of revolution bounded by a circular arc with a 3 m radius. Pressure transducers were used to measure a wave packet generated in the cone boundary layer by the freestream perturbation. Nine of these sensors formed three stations of azimuthal arrays and were used to determine the azimuthal variation of the wave packets in the boundary layer. The freestream laser-generated perturbation was positioned upstream of the model in three different configurations: along the centerline axis, offset from the centerline axis by 1.5 mm, and offset from the centerline axis by 3.0 mm. When the freestream perturbation was offset from the centerline of a flared cone with a 1.0 mm nose radius, a larger wave packet was generated on the side toward which the perturbation was offset. As a result, transition occurred earlier on that side. The offset perturbation did not have as large of an effect on the boundary layer of a nominally sharp flared cone.

Nomenclature

f	=	frequency, kHz
N	=	integrated growth factor
p	=	pressure, kPa
r_n	=	nose-tip radius, mm
Re/x	=	freestream unit Reynolds number, m^{-1}
T	=	temperature, K
t	=	time after tunnel starts, s
t_p	=	time after laser pulse is fired, ms
x	=	distance from nose tip, mm
ρ	=	density, kg/m^3

Subscripts

i	=	initial condition
s	=	surface condition
0	=	stagnation condition
∞	=	freestream condition

Superscript

$'$	=	fluctuation

I. Introduction

RECEPTIVITY is the manner in which freestream disturbances enter the boundary layer to initiate the growth of instabilities. Progress has been made in understanding the complex problem of laminar–turbulent boundary-layer transition, but work is still ongoing. Receptivity can introduce disturbances into a boundary layer via interactions of freestream disturbances with the leading-edge geometry, a discontinuity in surface curvature, and surface roughness [1]. Many computations of receptivity are performed for cases with small initial disturbances because the linear growth of instabilities is fairly well understood. These studies can involve the study of plane waves interacting with an axisymmetric or two-dimensional body [2–7] or the study of a discrete disturbance aligned to the axis of symmetry of a body [8]. Some theories have also been developed to show receptivity to freestream particulates [9] and entropy spots [10]. These theoretical and computational studies can provide great insight into the generation of boundary-layer instabilities by freestream disturbances, especially because the most unstable of instabilities tend to be axisymmetric or two-dimensional in high-speed flows. Fewer experimental studies of receptivity have been performed due to the difficulty in controlling the environment. High-speed experiments using a laser-generated disturbance have been performed in a quiet Mach 4 Ludwieg tube with the perturbation in the freestream [11,12], in a conventional Mach 6 Ludwieg tube with the perturbation deposited behind the shock [13], and in a quiet Mach 6 Ludwieg tube with the perturbation in the freestream [14].

Two-dimensional and axisymmetric disturbances are known to be the most unstable orientation of the second and higher modes of boundary-layer instabilities [15]. Thus, many computational and theoretical studies use the assumption of azimuthal periodicity or a reduction in dimensions to reduce computational cost. However, the alignment of discrete freestream disturbances to the body of a vehicle in flight may never be precise. Thus, it is important to study the effect of discrete, off-axis disturbances in the freestream and the nature of the boundary-layer instabilities that result. This type of study can require a large computational effort and cost, and so experimental investigations of this effect may help to provide direction for these studies.

McKenzie and Westphal theorized that the generation of vortical, acoustic, and thermal disturbances were possible once any of these three types of disturbances encountered an oblique shock [16]. The directionality of the generated disturbances is dependent upon the angle of incidence that the incoming disturbance has to the shock. The difference in angle of incidence and angle of transmission or generation is governed by Snell's law. Schilden et al. showed that the interaction of entropy waves with a shock could generate acoustic waves [17]. Schilden et al. also showed that the presence of

Presented as Paper 2015-1734 at the 53rd AIAA Aerospace Sciences Meeting, Kissimmee, FL, 5–9 January 2015; received 12 June 2017; revision received 29 November 2017; accepted for publication 21 December 2017; published online 21 February 2018.

*Research Aerospace Engineer, Flow Physics and Control Branch. Senior Member AIAA.

†Professor, School of Aeronautics and Astronautics. Associate Fellow AIAA.

incident acoustic and entropy waves generates circular pressure rings wrapped around a cone, which are caused by interference with the reflected wave. Previous computations by Dunn also show that the collision of a thermal spot with a hemispherical nose generates a vortex ring, which convects over a long period of time [18]. The convection period of this vortex ring along a hemisphere–cylinder geometry lasted well past any oscillations in the bow shock that may have resulted from the discrete freestream disturbance. More recent computations by Kianvashrad et al. [19,20] show that these vortex rings form as a result of the interaction between the laser-generated perturbation and that an off-axis laser-generated perturbation can form a larger vortex on the side toward which energy deposition occurs.

An important component of receptivity is the leading-edge geometry. Bluntness effects on receptivity and the growth of boundary layers have been investigated in several studies [4,21–23]. The receptivity of blunt bodies differs from that of sharper geometries due to the presence of an entropy layer. Computations shown by Balakumar and Kegerise [4] and Balakumar [7] indicate that the receptivity coefficient of a sharp nose to acoustic and vortical disturbances is orders of magnitude larger than on a blunt nose. On a blunt body, off-axis freestream disturbances first enter the entropy layer and do not enter the boundary layer until the entropy layer is swallowed by the boundary layer. Work by Balakumar [7] shows that, upstream of this swallowing location, acoustic disturbances do not grow in the boundary layer but instead act like trapped acoustic waves. Thus, for bodies with small bluntness (Reynolds number based on nose diameter less than 1000), the amplitude of the instability waves is smaller and transition is delayed because the start of growth is delayed.

The presence of instabilities in the boundary layer can cause an azimuthal variation in the fluctuating and mean components of boundary-layer properties. Several of these are periodic in nature and in the form of streamwise vortices or streaks [24–26]. A concave surface curvature generates the Görtler mode, which is important to geometries such as flared cones and nozzle walls. The Görtler instability typically manifests as counter-rotating pairs of stationary streamwise vortices. Li et al.'s computations showed the highest linear amplification of the stationary Görtler instability on a circular-arc flared cone had an azimuthal wave number of 50 and reached an N-factor of just under 6 at a unit Reynolds number of about $10 \times 10^6/\text{m}$ [27]. Previous work has shown that N-factors of approximately 5 are enough to cause transition in environments with significant amounts of freestream noise [28–30]. Other routes to transition were considered by Li et al., but the studies determined that the interaction of the Görtler and second-mode instabilities was the most likely interaction to initiate transition.

Azimuthal variation in the boundary layer may also be caused by the nonlinear growth of the primary boundary-layer instabilities. The nonlinear growth of the second-mode instability was investigated by Terwilliger [31], Sivasubramanian and Fasel [25,26], and again by Li et al. [32] for cones at Mach 6. The secondary instability of the second mode has a stationary vortex component and possibly accounts for the stationary vortices observed with temperature-sensitive paints in experiments at Purdue University [24,33]. Numerical studies by Sivasubramanian and Fasel [26] show that these streaks can be caused by the fundamental (K-type) or oblique nonlinear interactions of the second mode.

Past measurements of the receptivity of blunt bodies were performed in a Mach 4 quiet tunnel at Purdue University that has since been decommissioned [12,34,35]. A freestream laser-generated perturbation was positioned upstream of a hemisphere, and the response of the flowfield was measured with laser differential interferometry, a pressure transducer, and a schlieren system. Salyer noted that the impingement of the thermal disturbance on the hemisphere generated a rounded protrusion from the bow shock, indicative of a ring vortex [35]. The freestream perturbation used in Salyer's experiments contained both a thermal core and a weak shock, which arrived at the model at different times. The interaction of the bow shock from the hemisphere and the weak shock around the thermal perturbation appeared to generate a weak vortex ring. A stronger vortex ring was generated by the collision of the thermal disturbance and the bow shock, which was supported by Dunn's computations [18]. This indicates that the weak shock had some effect on the flowfield of the model, but the thermal disturbance had a larger effect. The effect of this vortex ring on the development of boundary-layer instabilities was not studied in either Salyer's or Dunn's work.

The experimental approach used in the study described in this paper was to create a controlled freestream perturbation in the Boeing/U.S. Air Force Office of Scientific Research (AFOSR) Mach 6 Quiet Tunnel (BAM6QT) at Purdue University. Characteristics of this perturbation were then measured with fast pressure transducer probes and presented in [36]. The perturbation was then allowed to convect downstream to a flared-cone model, where its effect was measured with surface-mounted pressure transducers. Measurements of the streamwise growth of instabilities generated by the freestream perturbation were presented in [14]. The present paper details the azimuthal measurements of the instabilities generated by the freestream laser perturbations. The freestream perturbation was placed along the same axis as the centerline of the cone and then later offset from the centerline axis to determine the effect of an off-axis freestream perturbation.

II. Facility and Equipment

The Boeing/AFOSR Mach 6 Quiet Tunnel (BAM6QT) at Purdue University is a Ludwieg tube that can be operated with laminar nozzle-wall boundary layers (Fig. 1). Conventional high-speed tunnels typically have turbulent nozzle-wall boundary layers that radiate acoustic noise into the freestream. These disturbances are not typically seen in flight and can cause transition to occur earlier in a ground-test facility. Quiet facilities have a reduced freestream acoustic noise level more comparable to flight [37–39] and provide a highly controlled environment in which receptivity can be studied carefully. More information about the development of such quiet tunnels can be found in [39].

In the BAM6QT, the acoustic noise level has been measured at around 0.02% for about the first 2 s of run time [40,41]. The operation of the tunnel creates an expansion wave that reflects between the end

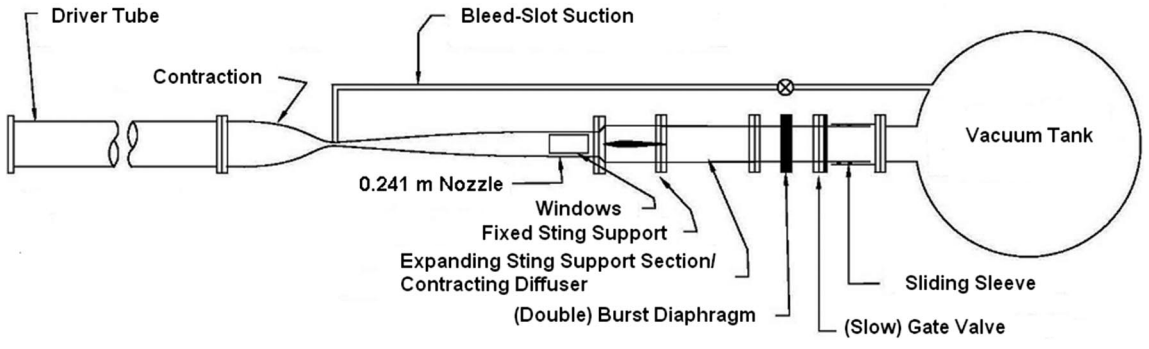

Fig. 1 Schematic of the Boeing/AFOSR Mach 6 Quiet Tunnel.

of the driver tube and the contraction about every 0.2 s. This reflection causes a stair-step decrease in the stagnation pressure, stagnation temperature, and unit Reynolds number. The decrease in stagnation pressure is less than 15%, and the decrease in stagnation temperature is about 4% over the first 2 s of the run. A model installed in the tunnel starts at room temperature and remains at about the same temperature during these short runs. After 2 s, the acoustic noise level increases slightly, and the run ends at about 4 or 5 s at the freestream conditions used for the experiment (Sec. II.D).

A. Laser Perturber

The laser perturber apparatus creates a perturbation in the freestream of a wind tunnel by focusing a high-powered Nd:YAG laser to a small volume. The apparatus consists of two main components: a Nd:YAG laser and a set of focusing optics designed by Collicott [42]. A Nd:YAG laser equipped with enhanced spatial mode and a laser seeder is used in this experiment. The beam diameter is about 4 mm. The maximum energy per pulse is typically around 270 mJ. The laser pulses are fired at a rate of 10 Hz, with each pulse lasting about 7 ns. The laser is frequency-doubled to output light at 532 nm.

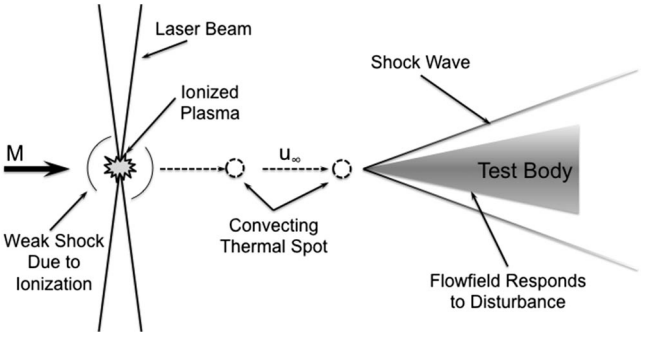

Fig. 2 Schematic of the streamwise position of the freestream perturbation relative to the test model.

An ionized plasma is created at the focus of the optical system via laser-induced breakdown. A multiphoton absorption process drives the laser-induced breakdown in low-density environments such as a wind tunnel [43]. The creation of the freestream perturbation through this process depends on the available molecules in the focal region as well as the photon flux. This plasma quickly cools within a few hundred nanoseconds, and a shock wave is emanated from the plasma core as it relaxes [19,44]. The perturbation generated in the freestream of the facility is a nearly spherical thermal perturbation surrounded by a weak, nearly spherical shock wave [12,45–47]. The shock dissipates fairly quickly, and so the shock is expected to have almost no effect on the flowfield of the model [11,12,45,48,49]. The thermal core is used as a controlled perturbation, which convects with the freestream and interacts with a test body downstream (Fig. 2). The perturbation can be generated upstream of the model either on the same axis as the model's centerline (Fig. 3a) or off the centerline (Figs. 3b–3d).

Measurements of the thermal disturbance were made with a pitot probe at different locations perpendicular to the beam axis of the laser perturber. The pitot pressure was measured with a fast pressure transducer with a 3.4 mm diameter and a resonant frequency greater than 1 MHz. The freestream measurements of the perturbation showed a nearly spherical perturbation lasting almost 9 μs and a deficit of 65% pitot pressure in the center of the perturbation. The size of this perturbation is approximately 6 mm [14,36]. The power spectra of these freestream measurements are given in Fig. 4. The spectral content at different locations across the laser perturbation indicate a decrease in the amplitude of the perturbation's effect as the probe is moved off of the centerline.

B. Flared-Cone Model

The model used for this experiment was a flared cone. The photograph of the model in Fig. 5 shows eight PCB sensors on the 0 deg ray toward the top of the page and three PCB sensors on the +120 deg ray on the bottom of the page. The geometry of the flared cone is a body of revolution bounded by a circular arc with a 3 m radius. The cone frustum was manufactured on a computer numerical

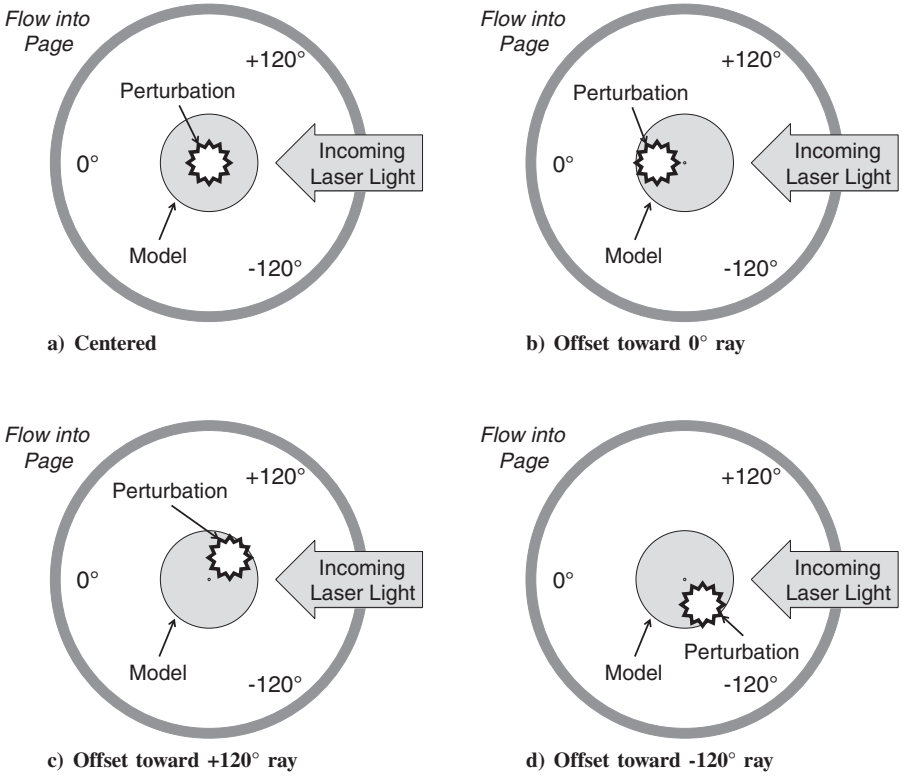

Fig. 3 Schematic of the spanwise position of the freestream perturbation relative to the test model.

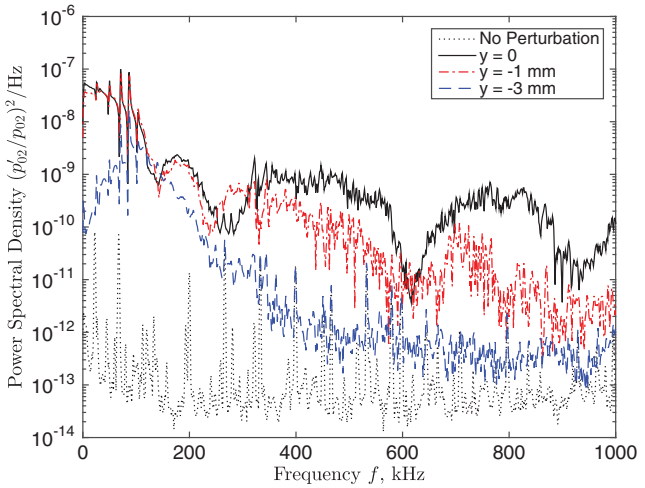

Fig. 4 Spectral content of the freestream laser-generated perturbation at locations on and off the centerline of the perturbation: $p_0 = 1022$ kPa, $T_0 = 412.8$ K, $\rho_\infty = 0.040$ kg/m^3.

Fig. 5 Photograph of the 3-m-circular-arc flared cone.

control lathe out of 6061-T6 aluminum round stock. The nose tips for the model are interchangeable and manufactured out of 17-4PH stainless steel round stock. A 1-mm-radius (blunt) nose tip and a 0.16-mm-radius (sharp) nose tip were used in this experiment. The nose tips are designed to be hemispherical, with the curvature of the nose tip laying tangent to the circular-arc flare. The sharp nose tip is 28 mm longer than the blunt nose tip, and so the position of the installed sensors relative to the nose tip changes with the change in nose tip.

A total of 14 PCB 132A31 fast pressure transducers were installed in the cone. Eight of these fast pressure transducers were installed along the 0 deg ray, which faced 180 deg away from the incoming Nd: YAG laser beam. Three sensors were installed on the +120 and −120 deg rays each to provide three axial rays and three stations of azimuthal sensor arrays. The azimuthal arrays of sensors were used both to align the cone model to the freestream and to study the azimuthal effects of the boundary-layer instabilities created by the laser-generated perturbation.

C. Data Acquisition

The data were recorded with three digital phosphor oscilloscopes, which can each record up to four different data channels. The maximum recording length of each of these channels is up to 250 million points. Two of the oscilloscopes have an analog bandwidth of 500 MHz, and one of the oscilloscopes has an analog bandwidth of 1 GHz. The sensors were sampled at 2 MHz for 5 s, the duration of a run. The data were acquired with the "high-res mode" feature on the oscilloscope, which samples the data at the maximum bandwidth and then filters and records the data at the user-specified sampling frequency.

D. Run Conditions

Run conditions for this model were limited to a small range of Reynolds numbers due to several factors. The initial stagnation temperature of the flow is nominally 433 K. The stagnation temperature of the flow drops about 4%, and the stagnation pressure drops less than 15% during the first 2 s of a run. Initial unit Reynolds numbers lower than about $Re_i/x = 5.3 \times 10^6$/m ($p_{0,i} = 500$ kPa) caused boundary-layer separation on the nozzle wall of the BAM6QT, due to tunnel blockage. Wave packets generated by the laser perturbation broke down at the aft end of the model for unit Reynolds numbers of about $Re/x = 7.1 \times 10^6$/m ($p_0 = 670$ kPa) on the sharp model and about $Re/x = 8.7 \times 10^6$/m ($p_0 = 820$ kPa) on the blunt model. For the blunt nose-tip model, unit Reynolds numbers lower than $Re/x = 7.1 \times 10^6$/m ($p_0 = 670$ kPa) produced small wave packets that were unable to be measured by most of the sensors along the length of the cone.

Conditions for the blunt flared cone and the sharp flared cone were chosen to provide similar boundary-layer states when there was no freestream laser perturbation present. The conditions were chosen so that the natural second-mode instability on the cone was to remain as linear as possible by the most-downstream measurement station, while still remaining large enough in amplitude to be measurable. These conditions were chosen in an attempt to keep the freestream laser perturbation from causing bypass transition. The choice to run the blunt flared cone at a unit Reynolds number of approximately 8×10^6/m allowed for the natural wave packet generated in the boundary layer to be large enough to be measurable at the last two azimuthal sensor stations without becoming turbulent. The choice to run the sharp flared cone at a unit Reynolds number of approximately 6×10^6/m was the lowest Reynolds number at the time that would allow the model to start without causing separation on the nozzle wall of the facility.

The position of the model nose tip relative to the initial location of the laser perturbation changes with each alignment of the focusing optics. The location where the laser perturbation is generated relative to the tip of the sharp nose tip varied from 92.4 to 113.6 mm between the different off-axis configurations detailed in Fig. 3. After the optics were aligned to position the perturbation at a certain off-axis position, the frustum of the model was held in a constant axial station, and only the nose tips were changed. Thus, the relative location of the blunt nose tip was 28 mm farther downstream than the sharp nose tip. The temperature of the thermal disturbance is expected to decay slightly in amplitude with time. The speed of the thermal disturbance is expected to be the same as the freestream velocity, which is nominally 874 m/s. The spherical shock speed is variable for the first microsecond but then slows down to the relative sound speed [19]. In the 28 mm difference between the nose tip, the thermal perturbation should experience little decay, whereas the weak spherical shock should dissipate before reaching either nose tip.

III. Azimuthal Measurements of a Wave Packet in the Boundary Layer

The azimuthal variation of the wave packet was studied by aligning the perturbation relative to the cone centerline in three different configurations. The perturbation was first aligned to the centerline axis and later offset by 1.5 and by 3.0 mm from the centerline axis. The offset from the centerline was positioned toward each ray of sensors, at azimuthal positions of 0, +120, and −120 deg. Similar effects were observed when the perturbation was offset toward the different rays of sensors, and so only the data with the perturbation offset toward the 0 deg ray are presented in this paper. The time traces corresponding to each sensor ray are offset by an amount proportional to the azimuthal position. The power spectral densities shown in this section are estimated using Welch's method to determine fast Fourier transforms (FFTs) of each wave packet, and 15 different FFTs are averaged together. The 95% confidence interval for this number of averages is approximately 0.1–5% of the maximum power in the expected second-mode frequency band, depending on the signal-to-noise ratio. The data are presented here with the time traces at each axial station in the left column of the figures, and the corresponding spectra to each of these time traces are presented in the right column.

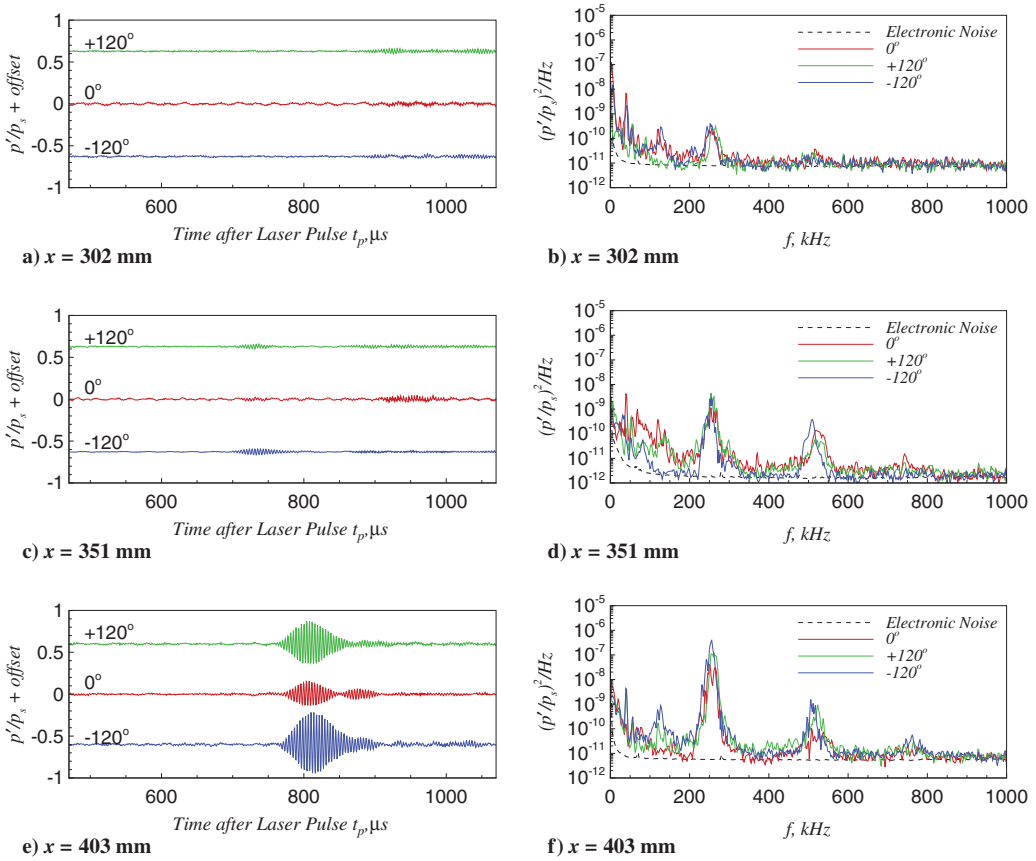

Fig. 6 Measured response to freestream laser perturbation on the blunt nose tip: $r_n = 1$ mm. $Re/x = 8.02 \times 10^6$/m. Perturbation is aligned to cone centerline.

A. Laser Perturbations Generated Along the Cone Centerline Axis

Figure 6 shows the time response and the power spectral densities of the measurements made on the blunt flared cone. The freestream perturbation was aligned to the cone centerline for the measurements shown. Figure 6a shows that the wave packets are not discernible from the natural second-mode waves at the first sensor station. The amplitude of the waves increases slightly around 850 μs after the laser pulse is fired. The cause of this increase is unknown because it appears at every sensor station at approximately the same time. The power spectra of the measurements at the most upstream azimuthal array ($x = 302$ mm) show a peak from the second-mode instability in at approximately 250 kHz (Fig. 6b). The wave packet becomes more apparent in the time traces starting at the second azimuthal array located at $x = 351$ mm at $t = 750$ μs but appears to be smaller on the 0 deg ray (Fig. 6c). The power spectra in Fig. 6d show that the first harmonic of the second mode is now present in all of the time traces at this axial station. Figure 6e shows that the wave packets grow larger as they travel downstream and are all about the same shape. The amplitudes of the wave packets are slightly different, which may result from a slight misalignment of the freestream disturbance relative to the cone centerline. The spectra in Fig. 6f show that the amplitudes and frequency bands for the second mode appear to be fairly similar around the azimuth at $x = 403$ mm.

Figure 7 shows the time response and power spectral densities of the measurements made on the sharp flared cone. Again, the freestream perturbation was aligned to the cone's centerline axis for these measurements. The wave packet is apparent in the time traces on the sharp cone at all three axial stations and at each azimuthal station. The vertical scaling of the time trace plots is 2.5 times the vertical scaling of the plots in Fig. 6 because the wave packets are much larger on the sharp flared cone than on the blunt flared cone, despite being at a lower Reynolds number. The first harmonic of the second mode is present in the power spectra of the measurements at the most upstream azimuthal array at $x = 332$ mm (Fig. 7b), indicating that the boundary-layer instability is already nonlinear at this measurement station. Higher harmonics appear in the spectra at the next azimuthal array at $x = 382$ mm (Fig. 7d). The presence of these large harmonics in each of the azimuthal arrays indicates that the wave packet may already be nonlinearly saturated at $x = 382$ mm. Furthermore, the wave packet may be fairly far along in the transition process at this point because the amplitude of the wave packet is large at approximately 9% of the computed surface pressure. However, there is no increase in the broadband noise, and so it does not appear that the wave packet has become turbulent. The harmonics begin to disappear from the spectra at the most downstream of the azimuthal arrays at $x = 434$ mm (Fig. 7f). The background frequency content also begins to rise, indicating that the wave packet has begun to break down near $x = 434$ mm.

B. Laser Perturbations Generated 1.5 mm Off of the Cone Centerline Axis

The freestream perturbation was next placed 1.5 mm off of the centerline axis and upstream of the model to determine the effect of a purposefully offset perturbation. This offset is approximately 25% of the diameter of the freestream perturbation, 75% of the blunt nose-tip diameter, and 469% of the sharp nose-tip diameter. Figure 8 shows the effect of this slightly offset perturbation on the instabilities generated in the boundary layer of the blunt flared cone. The perturbation is offset toward the 0 deg ray of sensors in these figures. As seen in Fig. 8a, the wave packet is not easily discernible from the natural second-mode waves at $x = 302$ mm on the blunt flared cone. Again, an unknown slight increase in amplitude is seen at about 850 μs after the laser pulse is fired, despite the fact that the position of the laser perturbation relative to the cone model has changed. A peak at the expected second-mode frequency (250 kHz) appears in the power spectra in Fig. 8b, indicating that any instabilities present are

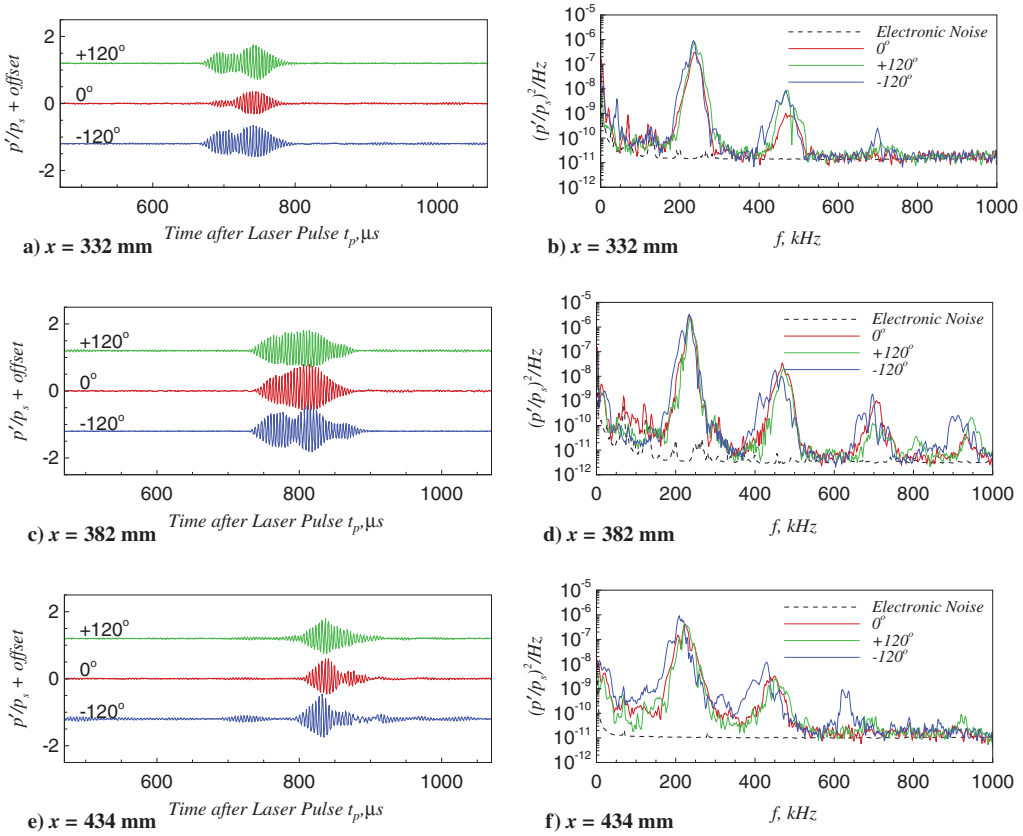

Fig. 7 Measured response to freestream laser perturbation on the sharp nose tip: $r_n = 0.16$ mm. $Re/x = 5.62 \times 10^6$/m. Perturbation is aligned to cone centerline.

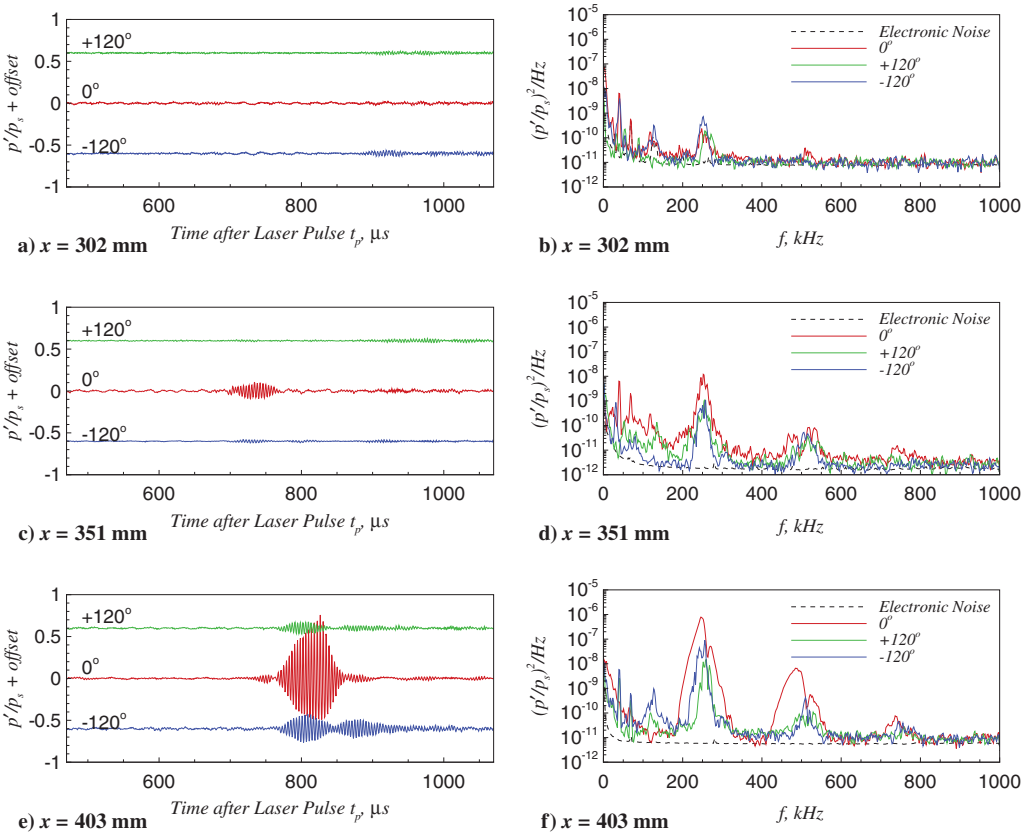

Fig. 8 Measured response to freestream laser perturbation on the blunt nose tip: $r_n = 1$ mm. $Re/x = 7.93 \times 10^6$/m. Perturbation is offset 1.5 mm from the cone centerline toward the 0 deg ray.

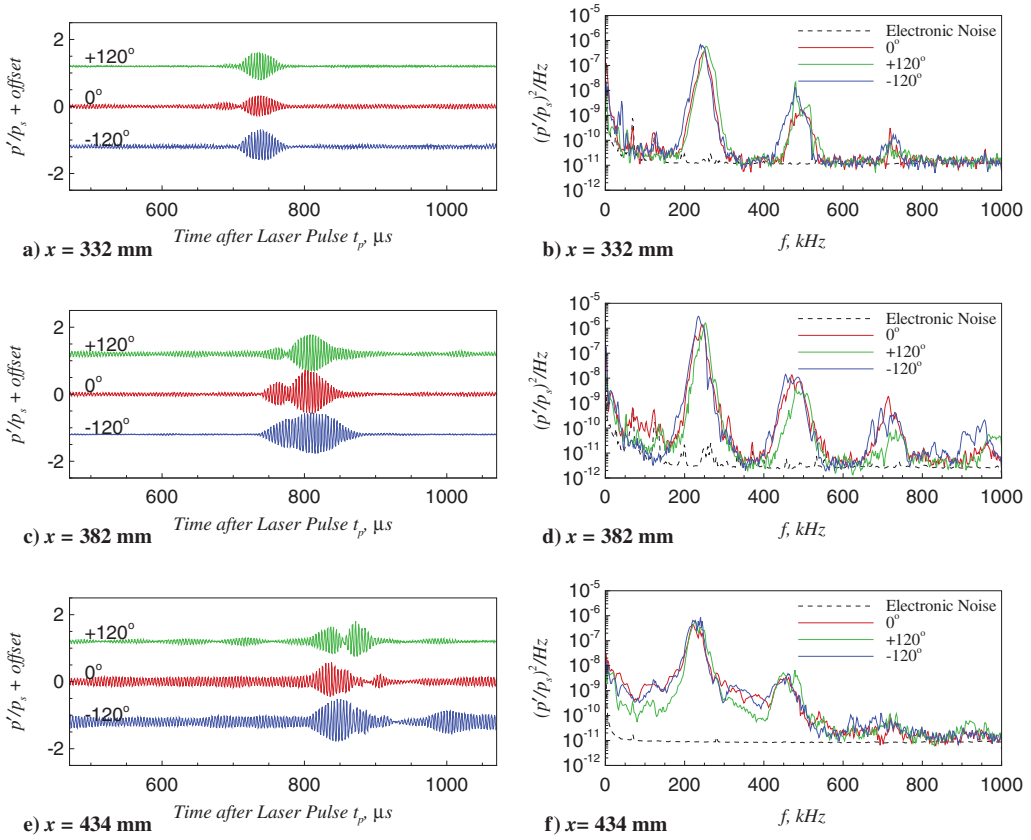

Fig. 9 Measured response to freestream laser perturbation on the sharp nose tip: $r_n = 0.16$ mm. $Re/x = 6.40 \times 10^6$/m. Perturbation is offset 1.5 mm from the cone centerline toward the 0 deg ray.

the same frequency as the natural second mode. At the next azimuthal sensor array at $x = 351$ mm, the wave packet on the 0 deg ray appears to be significantly larger than the wave packets on the +120 and −120 deg rays, which are barely discernible at this scaling. The power spectra in Fig. 8d indicate that the power in the second-mode instability is about an order of magnitude higher on the 0 deg rays than the other two rays. Finally, in the most downstream of the azimuthal arrays, the wave packet on the 0 deg ray is very large, whereas the wave packets on the +120 and −120 deg rays are similar in magnitude. The power spectra in Fig. 8f show that the power in the second-mode peak on the 0 deg ray is almost 1.5 orders of magnitude larger than on the other two rays. However, the power spectra in Fig. 8f do not indicate that the wave packet has begun to break down on the 0 deg ray. There are still clear peaks at the second-mode frequency band and at the first and second harmonics, but the peak second-mode frequency has decreased by approximately 8 kHz. The background broadband frequency content remains close to the electronic noise floor.

Figure 9 shows the effect of the offset perturbation on the sharp flared cone. Surprisingly, unlike the flow on the blunt flared cone, the wave packet in the boundary layer of the sharp flared cone does not appear to experience a change in amplitude with the change in perturbation position. Figure 9 shows the time traces from the three azimuthal sensor arrays. The shapes and amplitudes of the wave packets are similar, although some have an envelope for multiple bursts. The power spectra in Figs. 9b, 9d, and 9f all show that the second-mode frequency band has a large amplitude and the first and second harmonics are present. This indicates that the wave packets are nonlinearly saturated on the sharp flared cone by $x = 382$ mm and, again, that the wave packet on the sharp flared cone is further along the path to transition than on the blunt flared cone at this station. The power spectra in Fig. 9f show an increase in power in the lower frequencies on all three sensors at $x = 434$ mm. This increase is probably due to the beginning of breakdown of the wave packet.

C. Laser Perturbations Generated 3.0 mm Off of the Cone Centerline Axis

When the freestream perturbation was offset from the centerline by as much as 3.0 mm, its effect was more pronounced than when the offset was 1.5 mm. For reference, this offset corresponds to approximately 50% of the diameter of the freestream perturbation, 150% of the blunt nose-tip diameter, and 937% of the sharp nose-tip diameter. Figure 10 shows the time traces of the pressure fluctuations measured by the pressure sensors at the three different azimuthal arrays on the blunt flared cone. On the blunt flared cone, the wave packet on the 0 deg ray is similar to a turbulent spot. Instead of a smooth shape, the wave packet contains high- and low-frequency wavelengths and appears more jagged and sharp. This is the ray toward which the freestream perturbation is offset. The other sensors on the +120 and −120 deg rays show no sign of the wave packet at $x = 302$ mm (Fig. 10a), and a small wave packet is present at $x = 351$ mm and 403 mm (Figs. 10c and 10e). The power spectra show that there is a large amount of power in the broadband frequency content for each sensor along the 0 deg ray (Figs. 10b, 10d, and 10f). Thus, the frequency content of the wave packet on the 0 deg ray appears to resemble that of a turbulent spot even at the most upstream azimuthal array location of $x = 302$ mm. The power spectra for the sensors on the +120 and −120 deg rays show the second-mode peak and some harmonics with relatively low background frequency content, similar to when the perturbation was aligned to the cone centerline. Measurements made with the perturbation offset toward the +120 or −120 deg rays show a similar effect; the ray toward which the perturbation was placed has a turbulent spot, whereas the other rays show the presence of a coherent wave packet.

Figure 11 shows the time traces and the power spectra of the pressure fluctuations on the three different azimuthal arrays on the sharp flared cone. The wave packet on the sharp cone appears to be about the same shape and amplitude at each ray of sensors (Figs. 11a, 11c, and 11e) as in the previous cases. The power spectra also show

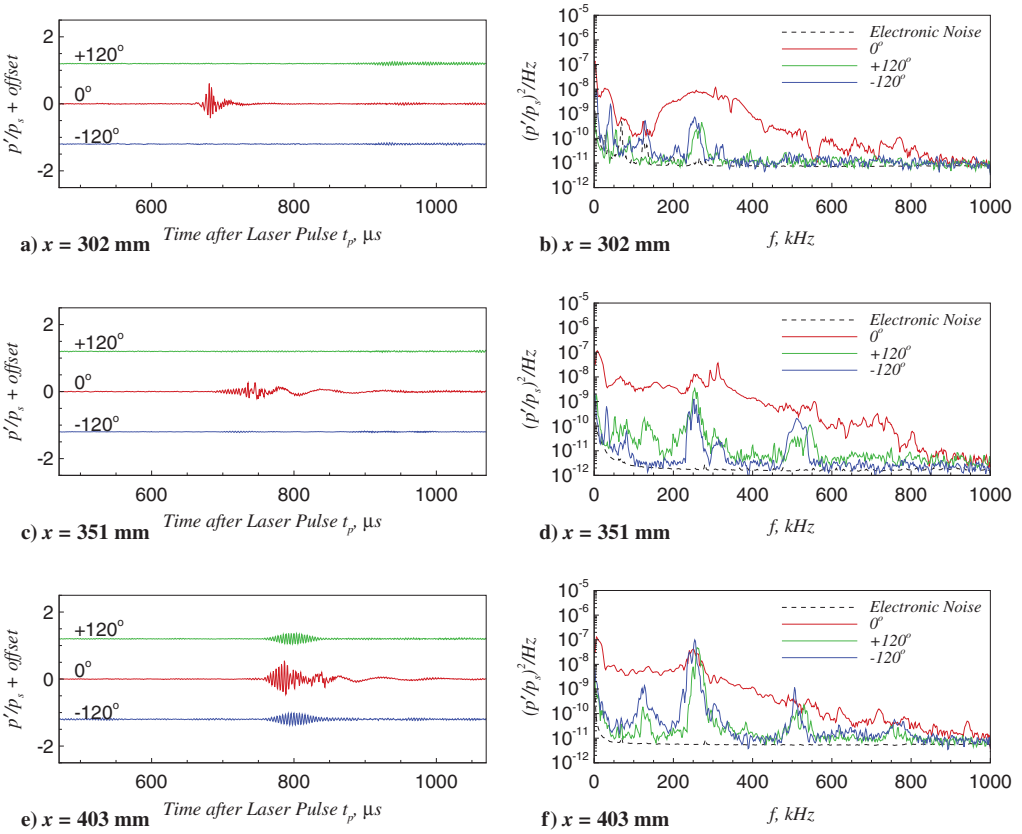

Fig. 10 Measured response to freestream laser perturbation on the blunt nose tip: $r_n = 1$ mm. $Re/x = 8.05 \times 10^6$/m. Perturbation is offset 3.0 mm from centerline toward the 0 deg ray.

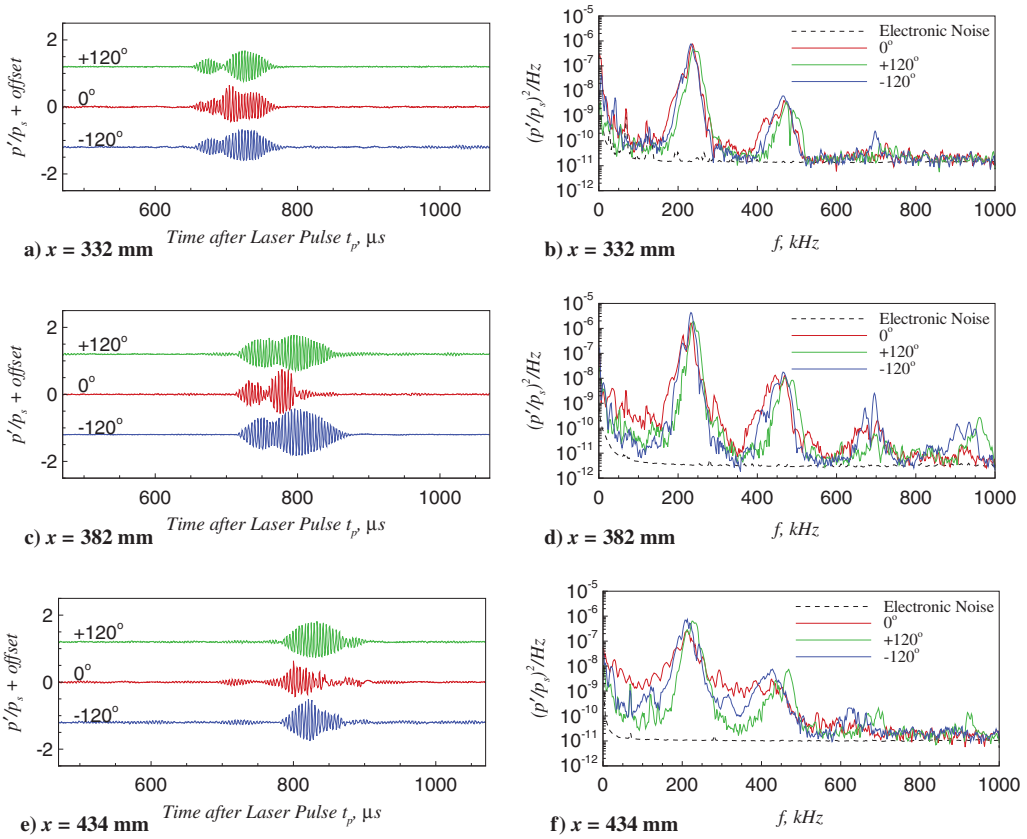

Fig. 11 Measured response to freestream laser perturbation on the sharp nose tip: $r_n = 0.16$ mm. $Re/x = 5.82 \times 10^6$/m. Perturbation is offset 3.0 mm from centerline toward the 0 deg ray.

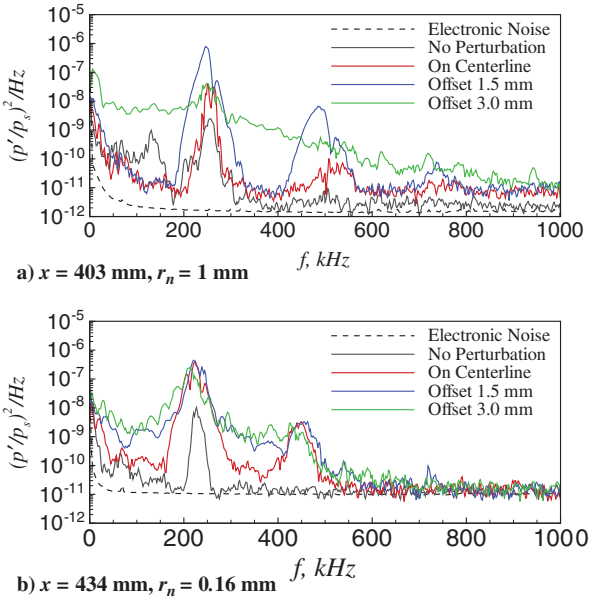

Fig. 12 Comparison of the power spectral density of measurements on the 0 deg ray at the last azimuthal sensor station with configurations of the freestream laser perturbation.

relatively similar amplitudes in the second-mode frequency band and in the higher harmonics (Figs. 11b, 11d, and 11f). However, there is some evidence that breakdown is starting to occur in the wave packet at $x = 434$ mm along the 0 deg ray; a broadband rise in the power of the lower frequencies between 0–450 kHz is shown in Fig. 11f for the sensor at 0 deg. The content in this 0–450 kHz frequency band at $+120$ and -120 deg is much less than at 0 deg. The larger offset perturbation has less of an effect on the sharp flared cone than on the blunt flared cone. For both offsets used in this experiment, the sharp nose tip appears to be less sensitive to the alignment of the freestream perturbation than the blunt nose tip.

D. Comparison of the Effect of the Laser Perturbation

Figure 12 shows a comparison of the power spectra for measurements taken at the last azimuthal sensor station on the 0 deg ray. Each plot shows the electronic noise, measurements with no laser perturbation in the freestream, measurements with the laser perturbation aligned to the centerline axis of the flared cone, measurements with the laser perturbation offset 1.5 mm from the centerline axis, and measurements with the laser perturbation offset 3.0 mm from the centerline axis. On the blunt flared cone, the amplitude of the natural second-mode instability increases in amplitude as the laser perturbation is added to the flow. Then, as the laser perturbation is farther offset from the centerline axis (Fig. 12a), the amplitude of the wave packet grows until the wave packet breaks down on the side toward which the perturbation was offset. At a 1.5 mm offset, the second-mode instability also appears to shift slightly in peak frequency. On the sharp flared cone, the presence of the freestream laser perturbation in the flow creates a larger-amplitude second-mode instability and a harmonic but otherwise does not change the broadband frequency content (Fig. 12b). There is a small increase in the broadband frequency content between 0 and 450 kHz when the freestream laser perturbation is offset from the centerline axis, but otherwise the second-mode instability and its harmonic appear to be of the same amplitude as when the laser perturbation is placed on the centerline.

IV. Discussion of the Measurements

As the freestream perturbation was shifted off the centerline axis of the blunt flared cone, the amplitude of the wave packet generated in the boundary layer also changed around the azimuth. Instead of generating an instability that was azimuthally uniform, the generated wave packet appeared to have larger amplitude on the side toward which the freestream disturbance was shifted. This phenomenon is observed in the computations in [20], which only focus on the vortex ring generation near the nose. Kianvashrad et al.'s work also deals with a freestream perturbation that is much smaller relative to the diameter of the model than in this experiment. However, the larger perturbation could have produced a similarly asymmetric vortex ring that generates an asymmetric disturbance in the boundary layer.

As the freestream perturbation shifted farther off the centerline axis of the blunt cone, the wave packet appeared to become larger on the side toward which the perturbation was offset. A shift of 3 mm off the model centerline caused breakdown of the wave packet at the first azimuthal sensor station on the ray toward which the laser perturbation was offset. The receptivity coefficient of the sharp flared cone to acoustic waves is 1.2, which is two orders of magnitude larger than the receptivity coefficient of the blunt flared cone, which is 9.3×10^{-3} [7]. Despite the expected higher receptivity in the sharp nose tip, the wave packet only appeared to be nonlinearly saturated at nearly all of the measurement stations on the sharp cone. Some evidence of spectral broadening was visible in the most downstream measurement station on the sharp flared cone (Fig. 12b), but unlike the blunt flared cone, the wave packet did not break down.

Streamwise alignment differences existed between the sharp cone and the blunt cone. The nose tip of the sharp flared cone was generally about 28 mm closer to the generation location of the perturbation than the blunt flared cone because the position of the model was not changed with respect to the location of the perturbation. This difference in generation location was a circumstance of working to ensure that the centerline axis of the cone remained stationary relative to the location of the perturbation between nose-tip changes. For a perturbation traveling at the nominal freestream flow speed of the BAM6QT, this distance is equivalent to about 32 μs difference in arrival time of the perturbation to the nose tip. Some decrease in the amplitude of the freestream perturbation has been noted in previous measurements in a different facility [36,50]. This decrease was up to 25–30% over the distance of 28 mm at $M = 3.5$ [36]. Regardless, this difference in streamwise distance between the nose tip and the location of the laser perturbation means that the sharp flared cone should experience a perturbation that is 25–30% larger in amplitude than the blunt flared cone.

Different Reynolds numbers were chosen for each nose tip to keep the natural second-mode instabilities as linear as possible along the length of the cone before introducing the freestream laser perturbation. In Fig. 12, no harmonic for the second mode was observed in the power spectra of measurements taken at the last measurement station for either nose tip when there was no freestream laser perturbation. However, the addition of a centerline laser perturbation on the sharp cone generated a wave packet that contains both the second mode and its harmonic frequency. In contrast, the centerline laser perturbation ahead of the blunt cone generated a wave packet that may become only weakly nonlinear by the most downstream measurement station. The generated wave packets on the sharp flared cone are fairly nonlinear at even the most upstream measurement station (Fig. 7b), whereas they are not for the blunt cone (Fig. 6b). Previous measurements have shown that the nonlinear growth region on the sharp flared cone could be very long, and so the fact that the wave packet remained nonlinear for the full length of the measurement region is not surprising [24,33]. The fact that the unit Reynolds number of the data on the sharp flared cone is 25% lower than the unit Reynolds number for the blunt flared cone may help to explain why the wave packet did not break down on the sharp flared cone. Matching the state of the natural boundary-layer instabilities on the flared cone may not be the correct way to compare the effects of nose bluntness for this experiment.

It is not clear why the amplitude of the wave packet on the sharp flared cone is not larger than on the blunt nose tip. It may be that the state of the initial disturbance in the boundary layer was different for each nose tip. The expected higher receptivity of the sharp nose tip caused the generated wave packet to be large-amplitude and nonlinear by the first measurement station when the laser perturbation was aligned to the cone centerline. The same configuration for the blunt cone created a much smaller-amplitude, linear wave packet, as expected. However, the 3-mm-offset perturbation on the blunt cone

generated a turbulent spot at the first measurement station (Fig. 10b), which indicates that the initial disturbance on the blunt flared cone was even larger for this configuration than it was for the sharp cone. Although the initial disturbance that generated the wave packet should be smaller on the blunt flared cone, it is possible that the effective amplitude of the perturbation becomes larger as it is shifted off of the centerline. Thus, a larger wave packet is created in the boundary layer of the blunt flared cone. Conversely, the laser perturbation on the centerline on the sharp flared cone generated a large, nonlinear wave packet, and so using the movement of the perturbation off-axis to create these same changes in effective amplitude may not have as much of an effect.

The off-axis disturbance may also be processed differently by the blunt flared cone than by the sharp flared cone. The shock in front of the blunt flared cone has a larger radius of curvature than the shock in front of the sharp flared cone. As a result, the entropy layer of the blunt flared cone may have some effect on the direction and magnitude of the disturbance as it enters the boundary layer. Without further measurements or computations of how this perturbation is processed by the flow around the flared cone, it is difficult to determine why the wave packets are larger on the blunt flared cone than on the sharp flared cone when the perturbation is generated off of the centerline axis.

V. Conclusions

These measurements show the azimuthal variation of a boundary-layer instability generated by a discrete freestream disturbance in a quiet tunnel. Measurements of the azimuthal variation of the boundary-layer instability on a flared cone were made with surface-mounted fast pressure transducers. The measurement of the azimuthal variation of the boundary-layer instabilities on a flared cone shows the uniformity, or lack thereof, in the generation of these wave packets. For a discrete freestream perturbation generated on the centerline axis of the tunnel, the effect on the boundary layer was fairly uniform around the azimuth. The confirmation of this effect is useful for assuming axisymmetry in complementary computations in that it allows for the reduction in dimensions.

The effect of the freestream laser perturbation on the nose tips changes with the bluntness. The wave packets generated by this disturbance on the sharp flared cone appeared to be large and nonlinear but never broke down to turbulence. The wave packets generated by the laser perturbation on the blunt flared cone appeared to be small and grew to larger amplitude. In some cases, the wave packets even became turbulent on the blunt flared cone, whereas the wave packets on the sharp flared cone remained nonlinearly saturated.

The blunt nose tip appears to be more sensitive to the alignment of the freestream perturbation to the centerline axis of the flared cone. Thus, it may be insufficient to know only the magnitude and frequency content of freestream disturbances, especially if some of these disturbances are discrete (e.g., entropy spots, particles). The geometry of the perturbation may be important, especially for blunt axisymmetric bodies. Slight modification of the position of the freestream perturbation relative to the centerline axis of the blunt flared cone appeared to change the amplitude of the instability wave packet on the ray toward which the perturbation was positioned. Similar effects of the offset perturbation are not observed on the sharp flared cone, indicating that the blunter body has a greater sensitivity to the position of the discrete freestream perturbation.

Acknowledgments

This research was funded by the U.S. Air Force Office of Scientific Research under grant FA9550-12-1-0167 and the NASA Pathways Intern Employment Program. Special thanks are given here to Steven H. Collicott for designing the laser perturbation-generating optical system and to Bradley M. Wheaton and Thomas J. Juliano for the initial design of the flared-cone model. Rolf Radespiel is acknowledged here for suggesting the use of an offset perturbation for these studies.

References

[1] Saric, W. H., Reed, H. L., and Kerschen, E. J., "Boundary-Layer Receptivity to Freestream Disturbances," *Annual Review of Fluid Mechanics*, Vol. 34, 2002, pp. 291–319. doi:10.1146/annurev.fluid.34.082701.161921

[2] Fedorov, A. V., "Receptivity of a High-Speed Boundary Layer to Acoustic Disturbances," *Journal of Fluid Mechanics*, Vol. 491, Sept. 2003, pp. 101–129. doi:10.1017/S0022112003005263

[3] Balakumar, P., "Receptivity of a Supersonic Boundary Layer to Acoustic Disturbances," *AIAA Journal*, Vol. 47, No. 5, May 2009, pp. 1069–1078. doi:10.2514/1.33395

[4] Balakumar, P., and Kegerise, M. A., "Receptivity of Hypersonic Boundary Layers over Straight and Flared Cones," *AIAA Journal*, Vol. 53, No. 8, Aug. 2015, pp. 2097–2109. doi:10.2514/1.J053432

[5] Balakumar, P., and Kegerise, M. A., "Receptivity of Hypersonic Boundary Layers to Acoustic and Vortical Disturbances," *49th AIAA Aerospace Sciences Meeting*, AIAA Paper 2011-0371, Jan. 2011.

[6] Balakumar, P., "Receptivity of Hypersonic Boundary Layers to Distributed Roughness and Acoustic Disturbances," *51st AIAA Aerospace Sciences Meeting Including the New Horizons Forum and Aerospace Exposition*, AIAA Paper 2013-0082, Jan. 2013.

[7] Balakumar, P., "Receptivity of Hypersonic Boundary Layers to Acoustic and Vortical Disturbances (Invited)," *45th AIAA Fluid Dynamics Conference*, AIAA Paper 2015-2473, June 2015.

[8] Huang, Y., and Zhong, X., "Numerical Study of Hypersonic Boundary-Layer Receptivity with Freestream Hotspot Perturbations," *AIAA Journal*, Vol. 52, No. 12, Dec. 2014, pp. 2652–2672. doi:10.2514/1.J052657

[9] Fedorov, A. V., "Receptivity of a Supersonic Boundary Layer to Solid Particulates," *Journal of Fluid Mechanics*, Vol. 737, Dec. 2013, pp. 105–131. doi:10.1017/jfm.2013.564

[10] Fedorov, A., Ryzhov, A. A., Soudakov, V., and Utyuzhnikov, S., "Receptivity of a High-Speed Boundary Layer to Temperature Spottiness," *Journal of Fluid Mechanics*, Vol. 722, May 2013, pp. 533–553. doi:10.1017/jfm.2013.111

[11] Schmisseur, J. D., Collicott, S. H., and Schneider, S. P., "Laser-Generated Localized Freestream Perturbations in Supersonic and Hypersonic Flows," *AIAA Journal*, Vol. 38, No. 4, April 2000, pp. 666–671. doi:10.2514/2.1008

[12] Salyer, T. R., Collicott, S. H., and Schneider, S. P., "Characterizing Laser-Generated Hot Spots for Receptivity Studies," *AIAA Journal*, Vol. 44, No. 12, Dec. 2006, pp. 2871–2878. doi:10.2514/1.13023

[13] Heitmann, D., and Radespiel, R., "Simulations of Boundary-Layer Response to Laser-Generated Disturbances at Mach 6," *Journal of Spacecraft and Rockets*, Vol. 50, No. 2, March–April 2013, pp. 305–316. doi:10.2514/1.A32282

[14] Chou, A., Balakumar, P., and Schneider, S. P., "The Development of Instabilities Generated by Freestream Laser Perturbations in a Hypersonic Boundary Layer," *AIAA Journal*, Vol. 55, No. 3, March 2017, pp. 799–807. doi:10.2514/1.J055280

[15] Mack, L. M., "Linear Stability Theory and the Problem of Supersonic Boundary-Layer Transition," *AIAA Journal*, Vol. 13, No. 3, March 1975, pp. 278–289. doi:10.2514/3.49693

[16] McKenzie, J. F., and Westphal, K. O., "Interaction of Linear Waves with Oblique Shock Waves," *Physics of Fluids*, Vol. 11, No. 11, Nov. 1968, pp. 2350–2362. doi:10.1063/1.1691825

[17] Schilden, T., Schröder, W., Ali, S. R. C., and Radespiel, R., "Interaction of Acoustic and Entropy Waves with Shocks," *44th AIAA Fluid Dynamics Conference*, AIAA Paper 2014-2352, June 2014.

[18] Dunn, J. W., "Numerical Simulation of Bow-Shock/Disturbance Interactions in Mach-4 Flows Past a Hemisphere," *36th AIAA Aerospace Sciences Meeting and Exhibit*, AIAA Paper 1998-0007, Jan. 1998.

[19] Kianvashrad, N., Knight, D., Wilkinson, S. P., Chou, A., Horne, R. A., Herring, G. C., Beeler, G. B., and Jangda, M., "Effect of Off-Body Laser Discharge on Drag Reduction of Hemisphere Cylinder in Supersonic Flow," *48th AIAA Plasmadynamics and Lasers Conference*, AIAA Paper 2017-3478, June 2017.

[20] Kianvashrad, N., Knight, D., Wilkinson, S. P., Chou, A., Horne, R. A., Herring, G. C., Beeler, G. B., and Jangda, M., "Effect of Off-Body Laser

Discharge on Drag Reduction of Hemisphere Cylinder in Supersonic Flow: Part 2," *2018 AIAA Aerospace Sciences Meeting*, AIAA Paper 2018-1433, Jan. 2018.

[21] Ericsson, L. E., "Effect of Nose Bluntness and Cone Angle on Slender-Vehicle Transition," *AIAA Journal*, Vol. 26, No. 10, Oct. 1988, pp. 1168–1174. doi:10.2514/3.10024

[22] Stetson, K. F., "Effect of Nose Bluntness and Cone Angle on Slender-Vehicle Transition," *AIAA Journal*, Vol. 28, No. 7, July 1990, pp. 1336–1337. doi:10.2514/3.25222

[23] Kara, K., Balakumar, P., and Kandil, O. A., "Effects of Nose Bluntness on Hypersonic Boundary-Layer Receptivity and Stability over Cones," *AIAA Journal*, Vol. 49, No. 12, Dec. 2011, pp. 2593–2606. doi:10.2514/1.J050032

[24] Berridge, D. C., Chou, A., Ward, C. A., Steen, L. E., Gilbert, P. L., Juliano, T. J., Schneider, S. P., and Gronvall, J. E., "Hypersonic Boundary-Layer Transition Experiments in a Mach-6 Quiet Tunnel," *48th AIAA Aerospace Sciences Meeting*, AIAA Paper 2010-1061, Jan. 2010.

[25] Sivasubramanian, J., and Fasel, H. F., "Direct Numerical Simulation of Transition in a Sharp Cone Boundary Layer at Mach 6: Fundamental Breakdown," *Journal of Fluid Mechanics*, Vol. 768, April 2015, pp. 175–218. doi:10.1017/jfm.2014.678

[26] Sivasubramanian, J., and Fasel, H. F., "Direct Numerical Simulation of Laminar–Turbulent Transition in a Flared Cone Boundary Layer at Mach 6," *54th AIAA Aerospace Sciences Meeting*, AIAA Paper 2016-0846, Jan. 2016.

[27] Li, F., Choudhari, M., Chang, C., Wu, M., and Greene, P. T., "Development and Breakdown of Görtler Vortices in High Speed Boundary Layers," *48th AIAA Aerospace Sciences Meeting*, AIAA Paper 2010-0705, Jan. 2010.

[28] Berridge, D. C., Casper, K. M., Rufer, S. J., Alba, C. R., Lewis, D. R., Beresh, S. J., and Schneider, S. P., "Measurements and Computations of Second-Mode Instability Waves in Several Hypersonic Wind Tunnels," *40th Fluid Dynamics Conference and Exhibit*, AIAA Paper 2010-5002, June 2010.

[29] Marineau, E. C., Moraru, C. G., Lewis, D. R., Norris, J. D., Lafferty, J. F., and Johnson, H. B., "Investigation of Mach 10 Boundary Layer Stability of Sharp Cones at Angle-of-Attack, Part 1: Experiments," *53rd AIAA Aerospace Sciences Meeting*, AIAA Paper 2015-1737, Jan. 2015.

[30] Marineau, E., "Prediction Methodology for Second-Mode-Dominated Boundary-Layer Transition in Wind Tunnels," *AIAA Journal*, Vol. 55, No. 2, Feb. 2017, pp. 484–499. doi:10.2514/1.J055061

[31] Terwilliger, N., "Numerical Investigation of Boundary Layer Instability Modes on a Compression Cone at Mach 6," M.S. Thesis, Dept. of Aerospace and Mechanical Engineering, Univ. of Arizona, Tucson, AZ, 2011.

[32] Li, F., Choudhari, M., Chang, C., and White, J., "Analysis of Instabilities in Non-Axisymmetric Hypersonic Boundary Layers over Cones," *10th AIAA/ASME Joint Thermophysics and Heat Transfer Conference*, AIAA Paper 2010-4643, June–July 2010.

[33] Chou, A., Ward, C. A., Letterman, L. E., Luersen, R. P., Borg, M. P., and Schneider, S. P., "Transition Research with Temperature-Sensitive Paint in the Boeing/AFOSR Mach-6 Quiet Tunnel," *41st AIAA Fluid Dynamics Conference and Exhibit*, AIAA Paper 2011-3872, June 2011.

[34] Salyer, T. R., Collicott, S. H., and Schneider, S. P., "Feedback Stabilized Laser Differential Interferometry for Supersonic Blunt Body Receptivity Experiments," *38th Aerospace Sciences Meeting and Exhibit*, AIAA Paper 2000-0416, Jan. 2000.

[35] Salyer, T. R., "Laser Differential Interferometry for Supersonic Blunt Body Receptivity Experiments," Ph.D. Thesis, School of Aeronautics and Astronautics, Purdue Univ., West Lafayette, IN, May 2002.

[36] Chou, A., Schneider, S. P., and Kegerise, M. A., "Characterization of a Laser-Generated Perturbation in High-Speed Flow for Receptivity Studies," *52nd Aerospace Sciences Meeting*, AIAA Paper 2014-0773, Jan. 2014.

[37] Schneider, S. P., "Flight Data for Boundary-Layer Transition at Hypersonic and Supersonic Speeds," *Journal of Spacecraft and Rockets*, Vol. 36, No. 1, Jan.–Feb. 1999, pp. 8–20. doi:10.2514/2.3428

[38] Schneider, S. P., "Effects of High-Speed Tunnel Noise on Laminar–Turbulent Transition," *Journal of Spacecraft and Rockets*, Vol. 38, No. 3, May–June 2001, pp. 323–333. doi:10.2514/2.3705

[39] Schneider, S. P., "Development of Hypersonic Quiet Tunnels," *Journal of Spacecraft and Rockets*, Vol. 45, No. 4, July–Aug. 2008, pp. 641–664. doi:10.2514/1.34489

[40] Juliano, T. J., "Nozzle Modifications for High-Reynolds-Number Quiet Flow in the Boeing/AFOSR Mach-6 Quiet Tunnel," M.S. Thesis, School of Aeronautics and Astronautics, Purdue Univ., West Lafayette, IN, Dec. 2006.

[41] Steen, L. E., "Characterization and Development of Nozzles for a Hypersonic Quiet Wind Tunnel," M.S. Thesis, School of Aeronautics and Astronautics, Purdue Univ., West Lafayette, IN, Dec. 2010.

[42] Collicott, S. H., "Initial Mach 6 LT Spot Maker Design Summary," Tech. Rept., Purdue Univ., West Lafayette, IN, Aug. 2010.

[43] Morgan, C. G., "Laser-Induced Breakdown Phenomena," *Science Progress*, Vol. 65, No. 257, Spring 1978, pp. 31–50.

[44] Ostrovskaya, G. V., and Zaĭdel', A. N., "Laser Spark in Gases," *Soviet Physics Uspekhi*, Vol. 16, No. 6, May–June 1974, pp. 834–855. doi:10.1070/PU1974v016n06ABEH004094

[45] McGuire, J. B., "Fluid Dynamic Perturbations Using Laser Induced Breakdown," M.S. Thesis, School of Aeronautics and Astronautics, Purdue Univ., West Lafayette, IN, Aug. 1994.

[46] Adelgren, R. G., Elliott, G. S., Knight, D. D., Zheltovodov, A. A., and Beutner, T. J., "Energy Deposition in Supersonic Flows," *39th Aerospace Sciences Meeting and Exhibit*, AIAA Paper 2001-0885, Jan. 2001.

[47] Heitmann, D., Radespiel, R., and Kähler, C., "Investigation of the Response of a Hypersonic Boundary Layer to Controlled Acoustic Disturbances," *48th AIAA Aerospace Sciences Meeting*, AIAA Paper 2010-0536, Jan. 2010.

[48] Yan, H., Adelgren, R., Boguszko, M., Elliott, G., and Knight, D., "Laser Energy Deposition in Quiescent Air," *AIAA Journal*, Vol. 41, No. 10, Oct. 2003, pp. 1988–1995. doi:10.2514/2.1888

[49] Limbach, C. M., and Miles, R. B., "Simultaneous Temperature, Density and Velocity Measurements in Laser-Generated Plasmas by Rayleigh and Filtered Rayleigh Scattering," *52nd Aerospace Sciences Meeting*, AIAA Paper 2014-0143, Jan. 2014.

[50] Chou, A., "Mach-6 Receptivity Measurements of Laser-Generated Perturbations on a Flared Cone," Ph.D. Thesis, School of Aeronautics and Astronautics, Purdue Univ., West Lafayette, IN, Aug. 2014.

B. Ganapathisubramani
Associate Editor